# Synthesis of $Li[(Ni_{0.5}Mn_{0.5})_{1-x}Li_x]O_2$ by Emulsion Drying Method and Impact of Excess Li on Structural and Electrochemical Properties

Seung-Taek Myung,*,† Shinichi Komaba,‡ Koutarou Kurihara,§ Kiyoharu Hosoya,§ Naoaki Kumagai,§ Yang-Kook Sun,|| Izumi Nakai,‡ Masao Yonemura,⊥ and Takashi Kamiyama⊥

*VK Corporation, 67 Jije-Dong, Pyongtaek-City, Kyonggi-Do 450-090, South Korea, Department of Applied Chemistry, Tokyo University of Science, 1-3 Kagurazaka, Shinjuku, Tokyo 162-8601, Japan, Department of Frontier Materials and Functional Engineering, Graduate School of Engineering, Iwate University, 4-3-5 Ueda, Morioka, Iwate 020-8551, Japan, Department of Industrial Chemistry, Hanyang University, Seoul 133-791, South Korea, and Neutron Science Laboratory, Institute of Materials Structure Science, High Energy Accelerator Research Organization, 1-1 Oho, Tsukuba, Ibaraki 305-0801, Japan*

*Received December 7, 2005. Revised Manuscript Received January 17, 2006*

Layered $Li[Ni_{0.5}Mn_{0.5}]O_2$ ($R\bar{3}m$ space group) was synthesized with controlling the Li/(Ni + Mn) ratio by employing an emulsion drying method, and the effect of Li on the transition-metal layer was investigated. Structural analyses of the final products were done by X-ray diffraction, neutron diffraction, and X-ray absorption near-edge spectroscopy. From the structural studies, we found that an excess amount of Li is located at the transition-metal layer and the presence of Li in the transition metal significantly improved structural ordering in the crystal structure. High capacity with good cyclability, faster $Li^+$ chemical diffusivity, less changes in the host structure by $Li^+$ de-/intercalation, and higher thermal stability were achieved for the Li-excess $Li[(Ni_{0.5}Mn_{0.5})_{0.94}Li_{0.06}]O_2$ compound relative to $Li[Ni_{0.5}Mn_{0.5}]O_2$. It is believed that such enhanced electrochemical properties are related to the improved physical and structural properties of Li-excess $Li[(Ni_{0.5}Mn_{0.5})_{0.94}Li_{0.06}]O_2$.

## Introduction

The $Li[Ni_{0.5}Mn_{0.5}]O_2$ system shows significant interesting electrochemical properties from the viewpoint of scientific and practical aspects.[1] The formal charges for the Ni and Mn of the material are 2+ and 4+, respectively.[2] Interestingly, only the $Ni^{2+/3+/4+}$ redox couples for $Li[Ni_{0.5}Mn_{0.5}]O_2$ are electrochemically available,[3] and they are accompanied by $Li^+$ intercalation. On the other hand, the tetravalent Mn remains electrochemically inactive, but it provides significant structural stability and shows single-phase transition during $Li^+$ de-/intercalation.[4]

Recently, we compared electrochemical properties of $Li[Ni_{0.5}Mn_{0.5}]O_2$ and $Li_{1.13}[Ni_{0.5}Mn_{0.5}]O_{2+z}$.[5] Though there was no large difference in the diffraction data, the resulting electrochemical properties of $Li_{1.13}[Ni_{0.5}Mn_{0.5}]O_{2+z}$ were superior to those of $Li[Ni_{0.5}Mn_{0.5}]O_2$; the capacity increase was shown to be approximately 25 mA h $g^{-1}$, and the extra capacity corresponds to the 0.1 mol of Li per unit in $Li[Ni_{0.5}Mn_{0.5}]O_2$. Shlyakhtin et al.[6] also reported similar results in the same system as ours, $Li_{1+x}[Ni_{0.5}Mn_{0.5}]O_{2+\delta}$ ($x = 0-0.2$). The phenomenon was even observed in Li-excess $Li_{1+x}[Ni_{1/3}Co_{1/3}Mn_{1/3}]O_2$, as suggested by Todorov and Numata.[7] Unfortunately, the origin of the superior electrochemical characteristics by Li excess was not clarified.

Such a $Li_{1+x}[Ni_{0.5}Mn_{0.5}]O_{2+\delta}$ composition can be written tentatively. In fact, however, the above chemical formula does not satisfy the layered $\alpha$-$NaFeO_2$ structure ($R\bar{3}m$ space group) because only 1 mol of Li and transition-metal per formula unit can occupy their own sites. Therefore, the following questions arise; first, does the excess amount of lithium incorporation into $Li[Ni_{0.5}Mn_{0.5}]O_2$ lead to the formation of impurities, such as $Li_2O$, $Li_2CO_3$, and so on? Second, if there is no impurity, where is the excess lithium located in the $Li[Ni_{0.5}Mn_{0.5}]O_2$ structure? Third, can the excess lithium be deintercalated from the host structure, resulting in a higher capacity? In the present study, we would like to discuss the synthesis and effect of the excess amount of Li on the structure and electrochemical properties of $Li[Ni_{0.5}Mn_{0.5}]O_2$.

* Author to whom correspondence should be addressed. Phone: +82-31-618-6000. Fax: +82-31-656-8073. E-mail: mstaek@vkcorp.co.kr.
† VK Corporation.
‡ Tokyo University of Science.
§ Iwate University.
|| Hanyang University.
⊥ High Energy Accelerator Research Organization.

(1) Ohzuku, T.; Makimura, Y. *Chem. Lett.* **2001**, *2001*, 744.
(2) Ueda, A.; Aoyama, S. *Proceeding of the 42th Battery Symposium in Japan*, Yokohama, Japan, 2001; p 130−131.
(3) Yoon, W.-S.; Grey, C. P.; Balasubramanian, M.; Yang, X.-Q.; McBreen, J. *Chem. Mater.* **2003**, *15*, 3161.
(4) Myung, S.-T.; Komaba, S.; Hosoya, K.; Hirosaki, N.; Miura, Y.; Kumagai, N. *Chem. Mater.* **2005**, *17*, 2427.
(5) Myung, S.-T.; Komaba, S.; Kumagai, N. *Solid State Ionics* **2004**, *170*, 139.
(6) Shlyakhtin, O. A.; Choi, S.-H.; Yoon, Y. S.; Oh, Y.-J. *J. Power Sources* **2005**, *141*, 122.
(7) Todorov, Y. M.; Numata, K. *Electrochim. Acta* **2004**, *50*, 495.

10.1021/cm052704j CCC: $33.50 
Published on Web 02/14/2006

## Experimental Section

$Li_{1+x}[Ni_{0.5}Mn_{0.5}]O_{2+\delta}$ powders were prepared by the emulsion drying method. We previously reported the details of the emulsion drying method.[8,9] The starting materials used for the synthesis of $Li_{1+x}[Ni_{0.5}Mn_{0.5}]O_{2+\delta}$ were $LiNO_3$ (Kanto), $Mn(NO_3)_2{\cdot}6H_2O$ (Kanto), and $Ni(NO_3)_2{\cdot}6H_2O$ (Kanto). In the starting emulsion, the atomic ratios of Li/(Ni + Mn) were 1−1.25. The obtained powder precursors were preliminarily annealed at 400 °C for 6 h in air, and they were then calcined at various temperatures in an air atmosphere. To remove the unreacted Li ingredient, the final products were thoroughly washed with distilled water and vacuum dried at 120 °C overnight. The chemical compositions of the resulting powders were analyzed by atomic absorption spectroscopy (AAS; Analyst 300, Perkin-Elmer).

X-ray diffractometry (XRD; Rigaku Rint 2200) was employed to characterize the prepared powders. XRD data were obtained at $2\theta = 10-100°$, with a step size of 0.03° and a count time of 5 s. The collected intensity data of XRD were analyzed by the Rietveld refinement program *Fullprof*.[10] Neutron powder diffraction of the $Li_{1+x}[Ni_{0.5}Mn_{0.5}]O_{2+\delta}$ powders was carried out at 295 K for ca. 5 h on the Sirius[11] time-of-flight neutron diffractometer at the pulsed spallation neutron facility at KENS, Japan. The samples were contained in a cylindrical V cell 9.2 mm in diameter, 20 mm in height, and 150 $\mu$m in thickness. An array of 320 $^3$He position-sensitive detectors (PSDs) installed in a backward bank with a $2\theta$ range from 145° to 175° was used to collect the intensity data. Incident neutron spectra were monitored with a $^3$He monitor counter. The difference in efficiency between the PSDs and the monitor counter was corrected using intensity data obtained in a separate measurement of incoherent scattering from V. The collected data were analyzed by the Rietveld refinement program RIETAN.[12] The Ni and Mn K-edge X-ray absorption near-edge structure (XANES) spectra of the as-prepared powders were measured in the transmission mode. The examinations were carried out at BL-12C, Photon Factory, KEK, Japan, using a Si(111) double-crystal monochromator. Nickel and manganese foils were used to calibrate the energies in each mode.

For fabrication of the positive electrodes, the prepared powders were mixed with acetylene black and polyvinylidene fluoride (80:15:5 in weight) in *N*-methylpyrrolidinon. The slurry thus obtained was coated onto Al foil and dried at 80 °C for 1 day for roll-pressing (500 kg $cm^{-2}$). About 10 mg was loaded onto the Al disk after punching (16 mm in diameter) for the cathode loading. The electrodes were dried again at 120 °C for 4 days in a vacuum state prior to use. A 2032 type of coin cell consisted of the cathode, lithium foil as an anode, and 1 M $LiPF_6$ in ethylene carbonate/diethyl carbonate (2:1 in volume) as an electrolyte. The cells were charged and discharged between 2.7 and 4.6 V versus Li by applying a current density of 20 mA $g^{-1}$ at 25 °C. For galvanostatic intermittent titration technique (GITT) measurement, a constant current flux was applied for a given time, followed by an open circuit for 10 h.

In situ XRD data were obtained using a Rigaku Rint 2200 diffractormeter from $2\theta = 10-70°$, with a step size of 0.03° and a count time of 7s. The in situ cell and attachment were fabricated by Rigaku, Inc., with a polypropylene film window fitted in the base of the cell to avoid the corrosion of a conventional beryllium window at higher potentials. The cell was charged and discharged with a current density of 20 mA $g^{-1}$. The lattice parameters were calculated by the following method: the positions of the individual peaks were fitted with a psuedo-Voigt or Lorentz function, and typically, 10 or 12 peak positions were input to minimize the least-squares difference between the calculated and measured peak positions by adjusting the lattice constant and the vertical displacement of the sample.

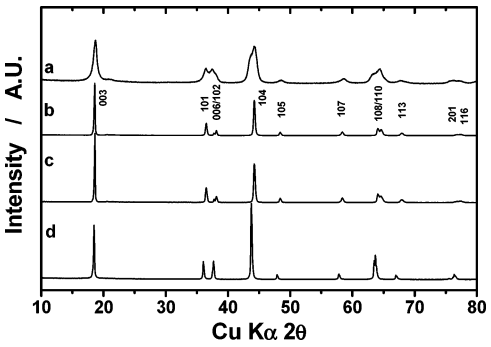


**Figure 1.** Phase evolution of Li−Ni−Mn−O compounds with increasing calcination temperature. (a) 400 °C for 6 h, (b) 650 °C for 12 h, (c) 800 °C for 12 h, and (d) 950 °C for 12 h in air. The starting ratio of Li/(Ni + Mn) = 1.0.

For differential scanning calorimetry (DSC) experiments, the cells were finally charged to 4.6 V and opened in the Ar-filled drybox. After opening the cell in the Ar-filled drybox carefully, the extra electrolyte was removed from the surface of the electrode, and the electrode materials were recovered from the current collector. A stainless steel sealed pan with a gold-plated copper seal (which can withstand 150 atm of pressure before rupturing and has a capacity of 30 $\mu$L) was used to collect 3∼5 mg samples. The measurements were carried out in a Pyris 1 Differential Scanning Calorimeter (Perkin-Elmer) using a temperature scan rate of 1 °C $min^{-1}$. The weight was constant in all cases, indicating that there were no leaks during the experiments.

## Results and Discussion

To synthesize $Li[Ni_{0.5}Mn_{0.5}]O_2$, selecting an appropriate synthetic method is important because even a small amount of Ni substitution for Mn sites (25%) in $Li[Ni_{0.5}Mn_{1.5}]O_4$ usually brought about undesirable secondary phases.[13] For the case of $Li[Ni_{0.5}Mn_{0.5}]O_2$, the ratio of Ni and Mn is 1:1 for the compound, which implies that the synthesis of $Li[Ni_{0.5}Mn_{0.5}]O_2$ would be much more difficult than that of $Li[Ni_{0.5}Mn_{1.5}]O_4$. As we previously reported, the emulsion drying method is one of the best methods to prepare substituted compounds, because it essentially gives a homogeneous powder precursor so that a simple heat treatment of the precursor led to high crystalline final products.[14] These trials and errors were employed to prepare homogeneous layered $Li[Ni_{0.5}Mn_{0.5}]O_2$.

Figure 1 shows the phase evolution of the emulsion-dried powder precursor with varying calcination temperatures in air. The starting ratio of Li/(Ni + Mn) was 1.00. As soon as

(8) Myung, S.-T.; Chung, H.-T.; Komaba, S.; Kumagai, N.; Gu, G.-H. *J. Power Sources* **2000**, *90*, 103.
(9) Myung, S.-T.; Komaba, S.; Kumagai, N. *J. Electrochem. Soc.* **2001**, *148*, A482.
(10) Roisnel, T.; Rodriguez-Carjaval, J. *Fullprof Manual*; Institut Laue-Langevin: Grenoble, France, 2000.
(11) Kamiyama, T.; Torii, S.; Mori, K.; Oikawa, K.; Itoh, S.; Furusaka, M.; Satoh, S.; Egami, T.; Ikeda, S.; Izumi, F.; Asano, H. *Mater. Sci. Forum* **2000**, *321−324*, 302.
(12) Izumi, F. In *The Rietveld Method*; Young, R. A., Ed.; Oxford University Press: Oxford, U. K., 1993; Chapter 13.
(13) Amine, K.; Tukamoto, H.; Yasuda, H.; Fujita, Y. *J. Electrochem. Soc.* **1996**, *143*, 1607.
(14) Myung, S.-T.; Komaba, S.; Hirosaki, N.; Kumagai, N.; Arai, K.; Kodama, R.; Nakai, I. *J. Electrochem. Soc.* **2003**, *150*, A1560.

**Table 1. Chemical Compositions of Li−Ni−Mn−O Compounds Varying Li/(Ni + Mn) Ratio, Calcination Temperature, and Calcination Time[a]**

| starting ratio of Li/(Ni + Mn) | calcination temperature (°C) | calcination time (hours) | final ratio of Li/(Ni + Mn) |
|---|---|---|---|
| 1 | 400 | 6 | 1.00 |
| 1 | 950 | 12 | 0.78 |
| 1.25 | 400 | 6 | 1.25 |
| 1.25 | 950 | 3 | 1.13 |
| | | 6 | 1.09 |
| | | 9 | 1.04 |
| | | 12 | 1.00 |

[a] The measurements were done by AAS.

the emulsion-dried precursor was fired at 400 °C for 6 h, a layer structure was formed due to the homogeneity of the emulsion-dried precursor, though the crystallinity is quite low in Figure 1a. An increase in the calcination temperature to 650 °C (Figure 1b) resulted in a more well-defined layered structure than that of Figure 1a, because one can observe the peak splittings of (006)/(102) and (108)/(110) pairs. Calcination at 800 °C for 12 h also led to improved crystallinity as seen in Figure 1c. The ratio of integrated intensity of $I_{003}/I_{104}$ was about 1.36, which is usually observable in α-$NaFeO_2$-type layer-structured compounds having a $R\bar{3}m$ space group.

However, a much higher calcination temperature brought about the inversion of the integrated intensity of $I_{003}/I_{104}$ in Figure 1d, which is derived from Li ingredient deficiency in the final product (Table 1). As seen in Table 1, approximately 0.22 mol per formula unit of Li were evaporated from the compound, leading to the final composition, Li/(Ni + Mn) = 0.78, by AAS. By observing the full width at half maximum of the (104) peaks, it is found that, although calcination of the emulsion-dried precursor at 800 °C led to phase-pure layer-structured material, calcination at 950 °C showed a much sharper (104) peak in Figure 1c and d, indicating higher crystallinity of the product. In fact, such a high crystallinity is essentially necessary to obtain good electrochemical properties, because the higher crystallinity provides improved structural integrity during repetitive $Li^+$ insertion and extraction. Therefore, a starting ratio of Li/(Ni + Mn) was decided to be 1.25 for the compensation of Li evaporated during calcination at 950 °C.

Figure 2 shows XRD patterns of the emulsion-dried precursor [Li/(Ni + Mn) = 1.25] calcined at 950 °C for given times in air. Unlike Figure 1d, when the starting ratio of Li/(Ni + Mn) was 1.0, calcination of the emulsion-dried precursor, which contains an excess amount of lithium salt, for 12 h resulted in a well-ordered layered structure having the $R\bar{3}m$ space group. The ratio of the integrated intensity of $I_{003}/I_{104}$ was about as high as 1.4. Surprisingly, only the 3 h calcination also produced the well-developed layer structure, as seen in Figure 2a. To observe the peak splittings of the (006)/(102) and (108)/(110) pairs, those peaks were magnified, and the corresponding XRD patterns are shown in Figure 2b and c. The peaks were clearly split, indicating the formation of a well-ordered α-$NaFeO_2$-type layered structure. Interestingly, reducing the calcination time resulted in the diffraction peak shifting toward a higher angle in $2\theta$. Varying the calcination time resulted in changes in the crystal structure, such as lattice constants. A reduced calcination

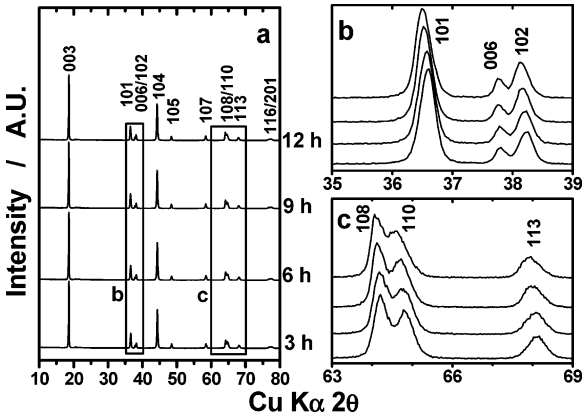


**Figure 2.** XRD patterns of Li−Ni−Mn−O compounds calcined at 950 °C with increasing calcination time. The starting ratio of Li/(Ni + Mn) = 1.25.

time obviously showed an increased Li/(Ni + Mn) ratio in the final products due to less evaporation of the Li ingredient during calcinations (Table 1).

As shown in Table 1, for example, one can see the final ratio of Li/(Ni + Mn) after calcination for 3 h to be 1.13 by AAS. On the basis of the chemical analysis, a chemical composition of $Li_{1.13}[Ni_{0.5}Mn_{0.5}]O_{2+z}$ is derived. Such an over-stoichiometry of Li does not satisfy the O3-type α-$NaFeO_2$ layer structure; 1 mole per formula unit of Li and transition-metal elements occupy 3*a* and 3*b* octahedral sites, respectively, which means that an excess amount of Li or other transition metal is not allowed in the structure. Because the final product was thoroughly washed with distilled water, as mentioned in the Experimental Section, the water soluble impurities should be removed. We speculated two possible ways to explain the condition of the excess Li in the composition: (i) the excess amount of Li can reside as impurities, such as $Li_2O$, $Li_2CO_3$, or $Li_2MnO_3$, with the final product, and (ii) the excess Li is located in the 3*b* octahedral site of the transition-metal layer. For the first proposition, those impurities are hardly detectable by using conventional XRD due to the poor X-ray scattering factor of Li. Therefore, neutron diffraction was employed to detect the Li-containing compound, as shown in Figure 3. As seen in the Li/(Ni + Mn) ratio of Table 1, one can find that a longer calcination (12 h) at 950 °C led to a stoichiometric composition, Li/(Ni + Mn) = 1.00 (Figure 3a). A neutron diffraction pattern of $Li_{1.13}[Ni_{0.5}Mn_{0.5}]O_{2+z}$ is shown in Figure 3b. Comparing the diffraction pattern with that of $Li[Ni_{0.5}Mn_{0.5}]O_2$, we can hardly observe any difference, and there are no impurities derived from $Li_2O$ and $Li_2CO_3$ in $Li_{1.13}[Ni_{0.5}Mn_{0.5}]O_{2+z}$.

To elucidate our second postulation, therefore, we performed a Rietveld refinement of the neutron diffraction data of $Li[Ni_{0.5}Mn_{0.5}]O_2$ and $Li_{1.13}[Ni_{0.5}Mn_{0.5}]O_{2+z}$ by assuming the space group $R\bar{3}m$. For the refinements, we supposed that the occupancy of each site was fixed to 1, $Ni^{2+}$ can be partly incorporated into the Li site, and the equivalent amount of Li can be introduced to the transition-metal site of $Ni^{2+}$ due to the similarity of the ionic radii of $Li^+$ (0.76 Å[15]) and $Ni^{2+}$ (0.69 Å[15]). The $Li_{1.13}[Ni_{0.5}Mn_{0.5}]O_{2+z}$ composition can be written with α-$NaFeO_2$ structure notation by our postulation,

(15) Shannon, R. D. *Acta Crystallogr., Sect. A* **1976**, *A32*, 751.

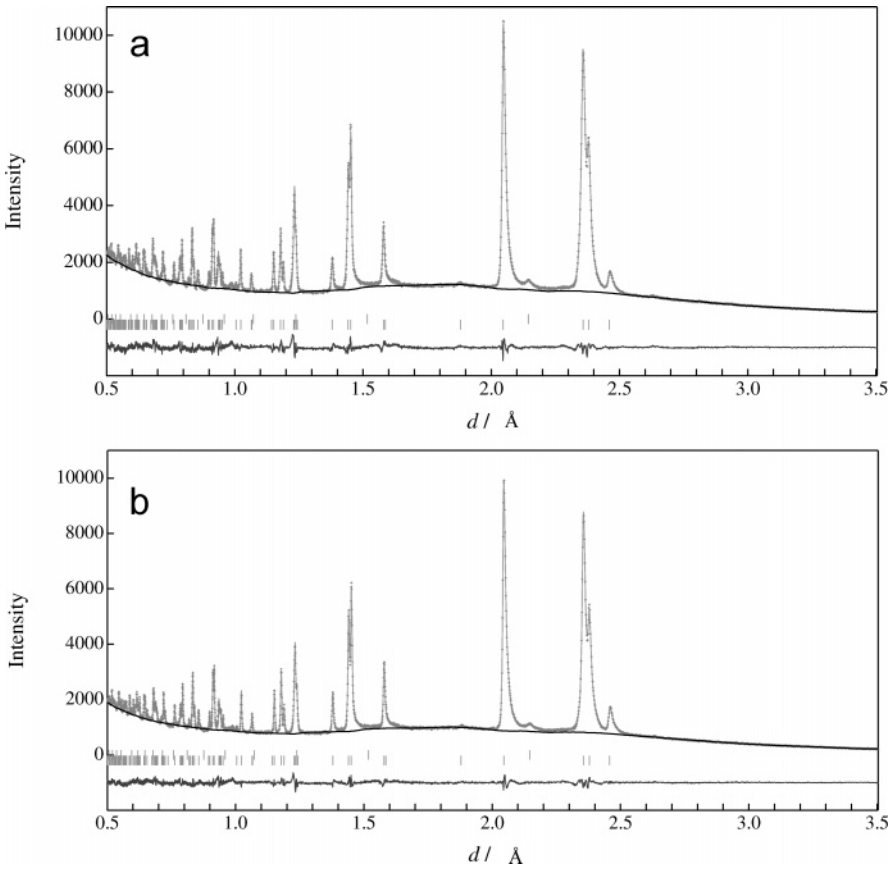


**Figure 3.** Neutron diffraction patterns of Li−Ni−Mn−O compounds calcined at 950 °C (a) for 12 h, final Li/(Ni + Mn) = 1.0, and (b) for 3 h, final Li/(Ni + Mn) = 1.13, determined by AAS.

**Table 2. Structural Parameters Obtained from Rietveld Refinement of the Neutron Diffraction Pattern of Li[Ni$_{0.5}$Mn$_{0.5}$]O$_2$ Calcined at 950 °C for 12 h in Air[a]**

| formula crystal system space group | | Li[Ni$_{0.5}$Mn$_{0.5}$]O$_2$ hexagonal *R*3*m* | | | | |
|---|---|---|---|---|---|---|
| element | site | *x* | *y* | *z* | *g* | *B* (Å$^2$) |
| Li1 | 3a | 0 | 0 | 0 | 0.927(2) | 2.208 |
| Ni2 | 3a | 0 | 0 | 0 | 0.073 | 2.208 |
| Ni1 | 3b | 0 | 0 | 1/2 | 0.427 | 0.503 |
| Mn1 | 3b | 0 | 0 | 1/2 | 0.500 | 0.503 |
| Li2 | 3b | 0 | 0 | 1/2 | 0.073 | 0.503 |
| O1 | 6c | 0 | 0 | 0.2420(9) | 1 | 0.921 |
| | $R_{wp}$ (%) | | | 5.31 | | |
| | $R_F$ (%) | | | 5.38 | | |
| | *S* | | | 2.8301 | | |

[a] The starting ratio of Li/(Ni + Mn) was 1.25.

**Table 3. Structural Parameters Obtained from Rietveld Refinement of the Neutron Diffraction Pattern of Li[(Ni$_{0.5}$Mn$_{0.5}$)$_{0.94}$Li$_{0.06}$]O$_2$ Calcined at 950 °C for 3 h in Air[a]**

| formula crystal system space group | | Li[(Ni$_{0.5}$Mn$_{0.5}$)$_{0.94}$Li$_{0.06}$]O$_2$ hexagonal *R*3*m* | | | | |
|---|---|---|---|---|---|---|
| element | site | *x* | *y* | *z* | *g* | *B* (Å$^2$) |
| Li1 | 3a | 0 | 0 | 0 | 0.974(30) | 5.397 |
| Ni2 | 3a | 0 | 0 | 0 | 0.026 | 5.397 |
| Ni1 | 3b | 0 | 0 | 1/2 | 0.443 | 0.453 |
| Mn1 | 3b | 0 | 0 | 1/2 | 0.470 | 0.453 |
| Li2 | 3b | 0 | 0 | 1/2 | 0.087 | 0.453 |
| O1 | 6c | 0 | 0 | 0.2415(7) | 1 | 0.818 |
| | $R_{wp}$ (%) | | | 4.67 | | |
| | $R_F$ (%) | | | 3.74 | | |
| | *S* | | | 2.8301 | | |

[a] The starting ratio of Li/(Ni + Mn) was 1.25.

as follows: [Li$_{(1-x)}$Ni$_x$]$_{3a}$[Ni$_{(1/2.13-x)}$Mn$_{1/2.13}$Li$_{(2.26/2.13-1+x)}$]$_{3b}$[O$_2$]$_{6c}$. From the structural model, Li$_{1.13}$[Ni$_{0.5}$Mn$_{0.5}$]O$_{2+z}$ can be expressed again as Li[(Ni$_{0.5}$Mn$_{0.5}$)$_{0.94}$Li$_{0.06}$]O$_2$. Hereafter, the Li-excess composition is referred to as Li[(Ni$_{0.5}$Mn$_{0.5}$)$_{0.94}$-Li$_{0.06}$]O$_2$.The refinements were done on the basis of chemical analysis results so that the occupancies were fixed during the refinements except those for the Li and Ni atoms due to the possibility of cation mixing between Li and Ni, and the corresponding neutron diffraction patterns of the Rietveld refinements of Li[Ni$_{0.5}$Mn$_{0.5}$]O$_2$ and Li[(Ni$_{0.5}$Mn$_{0.5}$)$_{0.94}$Li$_{0.06}$]-O$_2$ are shown in Figure 3 and in Tables 2 and 3, respectively. The refinements resulted in a good agreement between the observed and calculated patterns in Figure 3, which satisfies our structural model for the Li-excess composition. An interesting point concerns the site exchange of $Li^+$ and $Ni^{2+}$ between Li and the transition-metal layer. For the stoichiometric composition, Li[Ni$_{0.5}$Mn$_{0.5}$]O$_2$, 0.073 moles of the formula unit of $Ni^{2+}$ were incorporated into the Li layer. On the other hand, the $Ni^{2+}$ movement for Li[(Ni$_{0.5}$Mn$_{0.5}$)$_{0.94}$-Li$_{0.06}$]O$_2$ was quite reduced to 0.026 moles per formula unit, as described in Table 3. Neutron diffraction clearly indicates that the excess amount of Li did not lead to the formation of a Li[Ni$_{0.5}$Mn$_{0.5}$]O$_2$−Li$_2$MnO$_3$ solution, but the excess amount of Li is simply substituted for the transition-metal elements at the octahedral 3*b* site. Structural disorder in the 3*a* and 3*b* sites was also suppressed by Li introduction into the transition-metal layer in the crystal structure.

Figure 4 shows the Ni and Mn K-edge XANES spectra of the as-prepared Li[Ni$_{0.5}$Mn$_{0.5}$]O$_2$ and Li[(Ni$_{0.5}$Mn$_{0.5}$)$_{0.94}$-Li$_{0.06}$]O$_2$. The Ni spectra of the materials were compared with those of the spinel Li[Ni$_{0.5}$Mn$_{1.5}$]O$_4$ and layered LiNiO$_2$ in Figure 4a, where the average oxidations of Ni are 2+ and

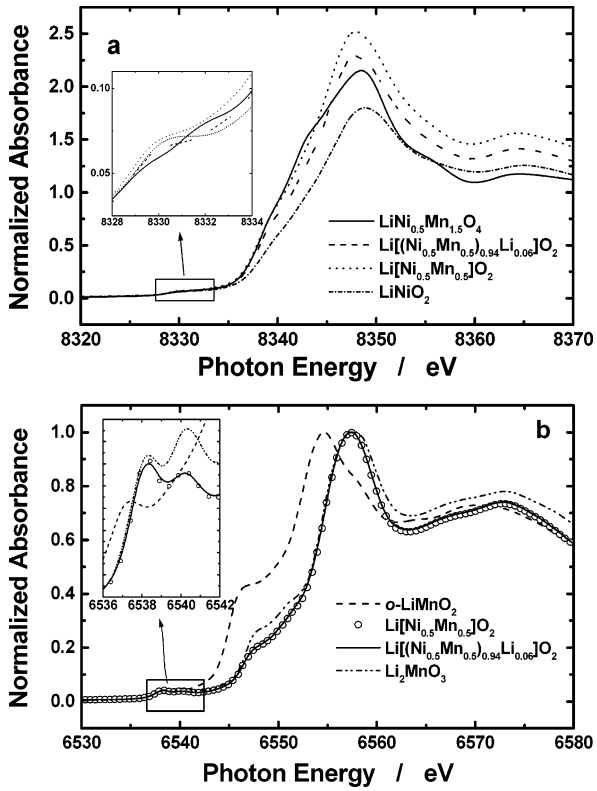


**Figure 4.** XANES spectra for $Li[Ni_{0.5}Mn_{0.5}]O_2$ and $Li[(Ni_{0.5}Mn_{0.5})_{0.94}Li_{0.06}]O_2$; (a) Ni K-edge spectra compared with $Li[Ni_{0.5}Mn_{1.5}]O_4$ and $LiNiO_2$; (b) Mn K-edge spectra compared with orthorhombic $LiMnO_2$ and rock salt $Li_2MnO_3$.

3+, respectively. The chemical shift in the XANES spectra has a positive correlation with the oxidation states of the absorber atom. As can be seen in Figure 4a, the main inflection (8320−8370 eV) of Ni for the $Li[Ni_{0.5}Mn_{0.5}]O_2$ is close to that of $Li[Ni_{0.5}Mn_{1.5}]O_4$. It suggests that the oxidation state of Ni in $Li[Ni_{0.5}Mn_{0.5}]O_2$ is close to 2+. However, the main inflection for the $Li[(Ni_{0.5}Mn_{0.5})_{0.94}Li_{0.06}]O_2$ is shifted slightly toward a higher position relative to the $Li[Ni_{0.5}Mn_{0.5}]O_2$ in Figure 4a. This result implies that the oxidation state of Ni in $Li[(Ni_{0.5}Mn_{0.5})_{0.94}Li_{0.06}]O_2$ is greater than that of $Li[Ni_{0.50}Mn_{0.5}]O_2$ but lower than that of $LiNiO_2$. The average oxidation states of Ni for both compounds were deduced by comparison with the chemical shifts of $Li[Ni_{0.5}Mn_{1.5}]O_4$ and layered $LiNiO_2$ from Figure 4a. By assuming the proportional relation between chemical shift and the average oxidation states of Ni for $Li[Ni_{0.5}Mn_{1.5}]O_4$ and $LiNiO_2$, the calculated oxidation state of Ni for $Li[Ni_{0.5}Mn_{0.5}]O_2$ was 2.2+ and that for $Li[(Ni_{0.5}Mn_{0.5})_{0.94}Li_{0.06}]O_2$ was 2.4+.

For Mn spectra, the as-prepared materials were compared with the layered orthorhombic $LiMnO_2$ and the rock-salt-type of $Li_2MnO_3$, where the oxidation states of Mn are 3+ and 4+, respectively, as seen in Figure 4b. The Mn K-edge spectra is practically identical to that of $Li_2MnO_3$, indicating that the Mn ion for both compounds is tetravalent and the coordination environments in the two compounds are close to each other. This suggests that Mn is almost in the tetravalent state with octahedral coordination. When the chemical shifts of $Li[Ni_{0.5}Mn_{0.5}]O_2$ and $Li[(Ni_{0.5}Mn_{0.5})_{0.94}Li_{0.06}]O_2$ are compared with those of the $LiMnO_2$ and $Li_2MnO_3$ by linear relation, the estimated Mn valences for both compounds were approximately 3.8+.

Lattice parameters of the as-prepared $Li[(Ni_{0.5}Mn_{0.5})_{1-x}Li_x]O_2$ ($x = 0-0.06$) were compared in Figure 5. With an increase in the Li content in the transition-metal layer, the *a*- and *c*-axis constants and unit volume decreased monotonically. As observed by XANES in Figure 4a, the oxidation state of Ni for $Li[(Ni_{0.5}Mn_{0.5})_{0.94}Li_{0.06}]O_2$ was slightly greater relative to that for $Li[Ni_{0.5}Mn_{0.5}]O_2$, which indicates that a greater amount of $Ni^{3+}$ is contained in $Li[(Ni_{0.5}Mn_{0.5})_{0.94}Li_{0.06}]O_2$ compared to $Li[Ni_{0.5}Mn_{0.5}]O_2$. When the ionic radii of $Ni^{2+}$ (0.69 Å[15]) and $Ni^{3+}$ (0.56 Å[15]) are taken into account, it is reasonable to think that the formation of the smaller $Ni^{3+}$ and the suppression of Ni/Li mixing by excess Li incorporation into the oxide matrix led to the linear decrease in the lattice parameter, as seen in Figure 5. Such a linear variation in the lattice parameter is usually observed in solid solution by following Vegard's law, suggesting that Li was readily substituted for the Ni and Mn. However, the *c*/*a* ratio did not change, though Li was incorporated in the transition-metal layer.

The existence of the smaller ion is also evidenced by the metal−oxygen distance of $Li[(Ni_{0.5}Mn_{0.5})_{1-x}Li_x]O_2$ ($x = 0$, 0.06), as seen in Table 4. Therefore, the interlayer distance is slightly greater for $Li[Ni_{0.5}Mn_{0.5}]O_2$. Dahn et al.[16] and Sun et al.[17] have shown that, when the amount of $Li_2MnO_3$ increased in $Li[Ni_{0.5}Mn_{0.5}]O_2$, the values of the lattice parameters became smaller compared to those of $Li[Ni_{0.5}Mn_{0.5}]O_2$, even though the *c*/*a* ratio significantly increased for the $Li_2MnO_3$-doped $Li[Ni_{0.5}Mn_{0.5}]O_2$. Provided that the solid solution of $Li[Ni_{0.5}Mn_{0.5}]O_2-Li_2MnO_3$ was formed, the calculated *c*/*a* value should increase by increasing the Li content in $Li[(Ni_{0.5}Mn_{0.5})_{1-x}Li_x]O_2$ ($x = 0-0.06$), as seen in Figure 5a. From this perspective, it is suggested that $Li[(Ni_{0.5}Mn_{0.5})_{1-x}Li_x]O_2$ ($x = 0-0.06$) would not lie on the tie line between $Li[Ni_{0.5}Mn_{0.5}]O_2$ and $Li_2MnO_3$, as confirmed by neutron diffraction in Figure 3b, because there are no changes in the Mn content of the final products, and no variations in the *c*/*a* ratio were observed in Figure 5 even though the Li content increased in the present work. As a result, we can briefly summarize the effect of Li in $Li[(Ni_{0.5}Mn_{0.5})_{1-x}Li_x]O_2$ ($x = 0-0.06$) on the structure: (i) the excess Li located at the transition-metal sites suppresses the structural disorder of both Li and transition-metal sites; (ii) an increase of the average oxidation state of Ni, in turn, compensates for the charge balance in the compound, compared with $Li[Ni_{0.5}Mn_{0.5}]O_2$, and (iii) the incorporation of Li into the transition-metal layer does not lead to the formation of a solid solution of $Li[Ni_{0.5}Mn_{0.5}]O_2-Li_2MnO_3$ but simply substitutes for Ni and Mn.

Figure 6 illustrates the initial charge and discharge curves of $Li[(Ni_{0.5}Mn_{0.5})_{1-x}Li_x]O_2$ ($x = 0-0.06$). The applied current density across the positive electrodes was 20 mA $g^{-1}$ at 25 °C. The charge curve of $Li[Ni_{0.5}Mn_{0.5}]O_2$ had a smooth voltage variation up to 4.6 V. On the other hand, even a small amount of Li introduction to the transition-metal layer had another voltage plateau above 4.4 V, as seen in Figure 6a. Derivation of the charge curve clearly indicates the

(16) Lu, Z.; Beaulieu, L. Y.; Donaberger, R. A.; Thomas, C. L.; Dahn, J. R. *J. Electrochem. Soc.* **2002**, *149*, A778.
(17) Shin, S.-S.; Sun, Y.-K.; Amine, K. *J. Power Sources* **2003**, *123*, 75.

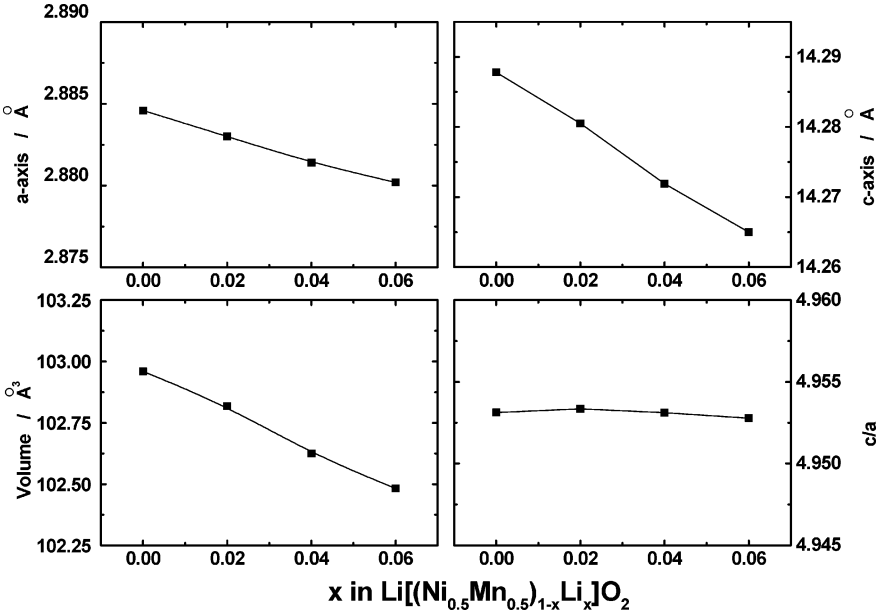


**Figure 5.** Variation in lattice parameters of Li[(Ni$_{0.5}$Mn$_{0.5}$)$_{1-x}$Li$_x$]O$_2$ ($x$ = 0−0.06). The obtained powders were calcined at 950 °C for a given time in air.

**Table 4. Metal−Oxygen Distances of Li[(Ni$_{0.5}$Mn$_{0.5}$)$_{1-x}$Li$_x$]O$_2$ ($x$ = 0 and 0.06) Calculated from Rietveld Refinements of Neutron Diffraction Results[a]**

| $x$ in Li[(Ni$_{0.5}$Mn$_{0.5}$)$_{1-x}$Li$_x$]O$_2$ | Li−O (Å) | M−O (Å) | MO$_2$ slab layer (Å) |
|---|---|---|---|
| 0 | 2.1168(6) | 1.9840(5) | 2.6147 |
| 0.06 | 2.1191(6) | 1.9779(6) | 2.6248 |

[a] M donates Ni and Mn. MO$_2$ = (2/3 − 2$z_{oxygen}$)$c$.

plateau in Figure 6b. Such a phenomenon is usually observed in Li-excess Li[Ni$_x$Li$_{(1/3-2x/3)}$Mn$_{(2/3-x/3)}$]O$_2$.[16,17] The obtained capacities of charge and discharge were also gradually increased by increasing the amount of Li in Li[(Ni$_{0.5}$Mn$_{0.5}$)$_{1-x}$Li$_x$]O$_2$. For example, the discharge capacity was increased approximately 25 mA h g$^{-1}$ for Li[(Ni$_{0.5}$Mn$_{0.5}$)$_{0.94}$Li$_{0.06}$]O$_2$, compared to that for Li[Ni$_{0.5}$Mn$_{0.5}$]O$_2$. These results would be ascribed to the extent of structural disorder, as we previously reported in Ti-doped Li[Ni$_{0.5}$Mn$_{0.5-x}$Ti$_x$]O$_2$.[4] As mentioned in Tables 2 and 3, the cation mixing in the crystal structure was significantly dependent on Li substitution in the transition-metal site, as was confirmed by neutron diffraction. Therefore, the Li-substituted Li[(Ni$_{0.5}$Mn$_{0.5}$)$_{1-x}$Li$_x$]O$_2$, especially where $x$ = 0.06, had a much higher capacity than Li[Ni$_{0.5}$Mn$_{0.5}$]O$_2$.

Li substitution for Ni and Mn sites, Li[(Ni$_{0.5}$Mn$_{0.5}$)$_{0.94}$Li$_{0.06}$]O$_2$, also showed a slight decrease in the polarization at the beginning of Li$^+$ extraction, as seen in Figure 6a. Upon discharge, however, the operation voltage was about 0.1 V higher for the entire range in Figure 6a and b. It is well-known that the presence of Ni$^{2+}$ in the Li layer disturbs Li$^+$ de-/intercalation.[18] The reduced structural disorder by the Li substitution resulted in a slight increase in the operation voltage upon discharge in Figure 6b, which means that a smaller polarization between charge and discharge was seen by the Li substitution in Li[(Ni$_{0.5}$Mn$_{0.5}$)$_{0.94}$Li$_{0.06}$]O$_2$.

Figure 7 shows the continuous charge and discharge curves of Li[Ni$_{0.5}$Mn$_{0.5}$]O$_2$ and Li[(Ni$_{0.5}$Mn$_{0.5}$)$_{0.94}$Li$_{0.06}$]O$_2$. For Li[Ni$_{0.5}$Mn$_{0.5}$]O$_2$, the capacity faded gradually as the cycle went by. In addition, the operation voltage dropped gradually during cycling. On the other hand, Li[(Ni$_{0.5}$Mn$_{0.5}$)$_{0.94}$Li$_{0.06}$]O$_2$ retained its initial capacity well during 50 cycles, and the capacity retention was approximately 95%. The Li/Li[(Ni$_{0.5}$Mn$_{0.5}$)$_{0.94}$Li$_{0.06}$]O$_2$ cell also showed much less of a decrease in the operation voltage upon cycling. It is likely that such results are related to the cation mixing of the final product.

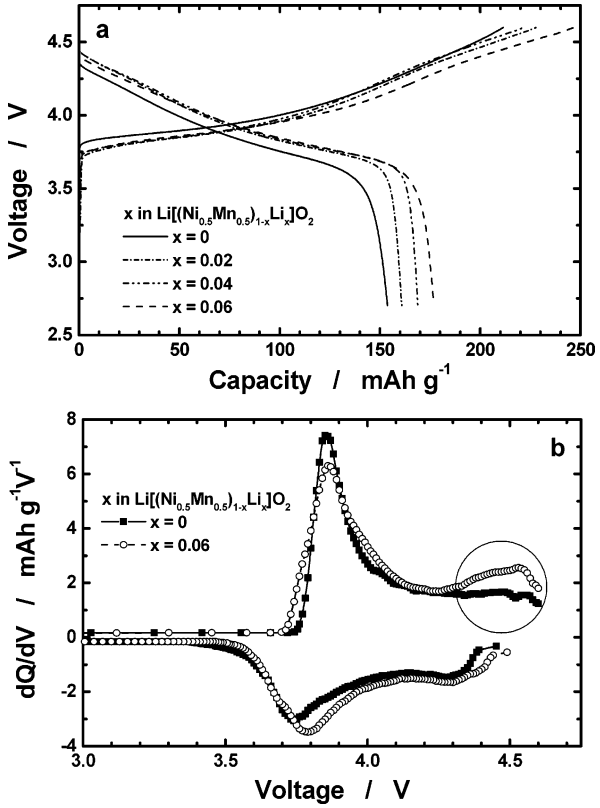


**Figure 6.** (a) Initial charge and discharge curves of Li/Li[(Ni$_{0.5}$Mn$_{0.5}$)$_{1-x}$Li$_x$]O$_2$ ($x$ = 0−0.06) cells and (b) their differentiated curves for Li/Li[(Ni$_{0.5}$Mn$_{0.5}$)$_{1-x}$Li$_x$]O$_2$ ($x$ = 0 and 0.06) cells. The applied current density across the positive electrode was 20 mA g$^{-1}$ at 25 °C.

(18) Pouillerie, C.; Croguennec, L.; Biensan, P.; Willmann, P.; Delmas, C. *J. Electrochem. Soc*. **2000**, *147*, 2061.

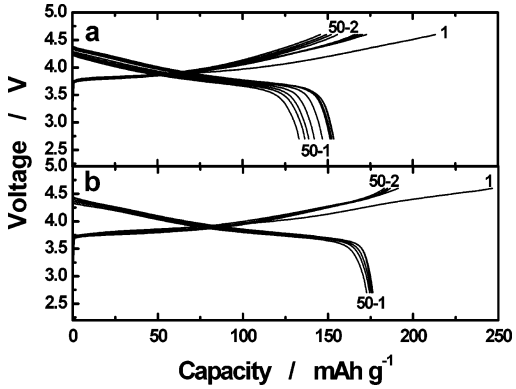


**Figure 7.** Continuous charge and discharge curves of (a) Li/Li[$Ni_{0.5}Mn_{0.5}$]-$O_2$ and (b) Li/Li[$(Ni_{0.5}Mn_{0.5})_{0.94}Li_{0.06}$]$O_2$ cells. The applied current density across the positive electrode was 20 mA $g^{-1}$ at 25 °C.

As reported previously by Delmas' group,[18,19] in the $Li_xNiO_2$ system, the dramatic deterioration of the electrochemical performances was strongly related to the $Ni^{2+}$ ion occupied in the Li layer, which induces a local collapse of the structure and hinders not only lithium diffusion in the interslab but also lithium reintercalation. For this reason, the operation voltage was decayed during repetitive $Li^+$ de/-intercalation, and this, in turn, caused capacity fading for the Li[$Ni_{0.5}Mn_{0.5}$]-$O_2$, as seen in Figure 7a. For Li[$(Ni_{0.5}Mn_{0.5})_{0.94}Li_{0.06}$]$O_2$, which had a much reduced $Ni^{2+}$ occupation in the Li layer compared to Li[$Ni_{0.5}Mn_{0.5}$]$O_2$, on the other hand, it is likely that disturbance of the $Li^+$ insertion or extraction is less severe than that for Li[$Ni_{0.5}Mn_{0.5}$]$O_2$ due to the improved structural ordering, so that it could retain the high capacity with a much reduced voltage decay during cycling, as seen in Figure 7b.

In situ XRD measurements were carried out to understand the structural changes of the active materials and their dependences on the Li contents. The first charge and discharge curves are given, and the measurements were done at the circle-marked points shown in Figures 8a and 9a. The diffraction peaks of stainless exmet (revealed as S) are used as the internal standard, and the corresponding patterns are shown in Figures 8b and 9b.

As $Li^+$ deintercalated from the host structure, (00*l*) peaks were gradually shifted toward a lower angle until $\delta$ was 0.6 in $Li_{1-\delta}[Ni_{0.5}Mn_{0.5}]O_2$ (Figure 8b) and $Li_{1-\delta}[(Ni_{0.5}Mn_{0.5})_{0.94}Li_{0.06}]O_2$ (Figure 9b). Then, the peaks were moved to a higher angle in the first charge stage. On the other hand, all other peaks were shifted smoothly toward a higher angle in $2\theta$ during the first charge without any peaks of secondary phases in the XRD pattern. Broadening of the (003) and (018) peaks can be observed from $\delta = 0.4$ in $Li_{1-\delta}[Ni_{0.5}Mn_{0.5}]O_2$ and $Li_{1-\delta}[(Ni_{0.5}Mn_{0.5})_{0.94}Li_{0.06}]O_2$ in Figures 8b and 9b, respectively. The broadening of the diffraction lines suggests that local inhomogeneities occur due to fluctuations of the cationic distribution in the interslab spaces. In addition, when $\delta = 0.4$ in $Li_{1-\delta}[Ni_{0.5}Mn_{0.5}]O_2$ and $\delta = 0.5$ in $Li_{1-\delta}[(Ni_{0.5}Mn_{0.5})_{0.94}Li_{0.06}]O_2$, one can see a minor change in the diffraction pattern in which the (006) peak is merged with the (102) peak upon the charge, as seen in Figures 8b and 9b, respectively. The

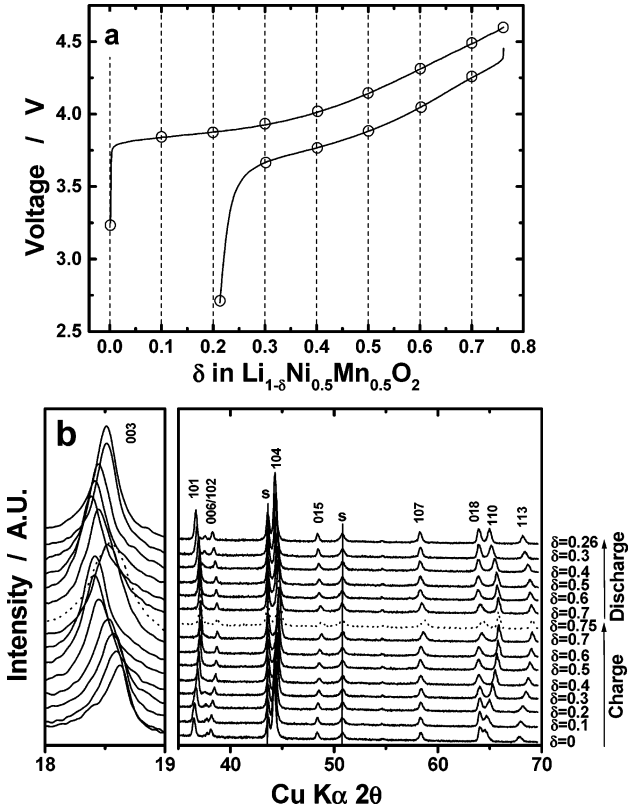


**Figure 8.** (a) Charge and discharge curves of the initial cycle for the Li/$LiNi_{0.5}Mn_{0.5}O_2$ cell. In situ XRD measurements were carried out at the position marked by the circles. (b) In situ XRD patterns of $Li_{1-\delta}Ni_{0.5}Mn_{0.5}O_2$ as a function of Li content during the first cycle. S donates a stainless exmet for loading active materials, and the exmet was used as the internal standard for calibration.

reversible behaviors were seen during the discharge, which means that a single-phase reaction occurred topotactically during $Li^+$ de-/intercalation. Obviously, there is no large difference in the in situ XRD patterns for $Li_{1-\delta}[Ni_{0.5}Mn_{0.5}]O_2$ and $Li_{1-\delta}[(Ni_{0.5}Mn_{0.5})_{0.94}Li_{0.06}]O_2$.

From the in situ XRD patterns in Figures 8 and 9, lattice parameters were calculated by a least-squares method and the results are given in Figure 10. All partial de-/intercalated phases remain isotypic with the starting material and can, therefore, be indexed in the $R\bar{3}m$ space group, showing that an overall solid solution exists during $Li^+$ de/intercalation. Differences in *a* and *c* axes and unit volume ($\Delta a$, $\Delta c$, and $\Delta V$, respectively) during the first cycle were used for comparison. As $Li^+$ ions were extracted from the host structure, the *a* axis decreased monotonically, which corresponds to the reduction of the metal−metal interslab distance, because the ionic radii of $Ni^{3+}$ and $Ni^{4+}$ formed during the charge are smaller than that of $Ni^{2+}$. This, therefore, leads to a decrease in metal−oxygen distance and an increase in covalency, especially at the highly delithiated state. The reverse variations in the *a* axis were seen upon the intercalation process. However, the values did not return to their original states due to the irreversible reaction in the charge process. The *c*-axis constants increased in the following deintercalations of $Li_{1-\delta}[Ni_{0.5}Mn_{0.5}]O_2$ and $Li_{1-\delta}[(Ni_{0.5}$-$Mn_{0.5})_{0.94}Li_{0.06}]O_2$: the *c* axis increases due to the stronger oxygen−oxygen electrostatic repulsions through the interslab space when the $Li^+$ ions are removed. The observed decrease in the *c* axis shows that the structure becomes covalent

(19) Delmas, C.; Saadoune, I.; Rougier, A. *J. Power Sources* **1993**, *43*−*44*, 595.

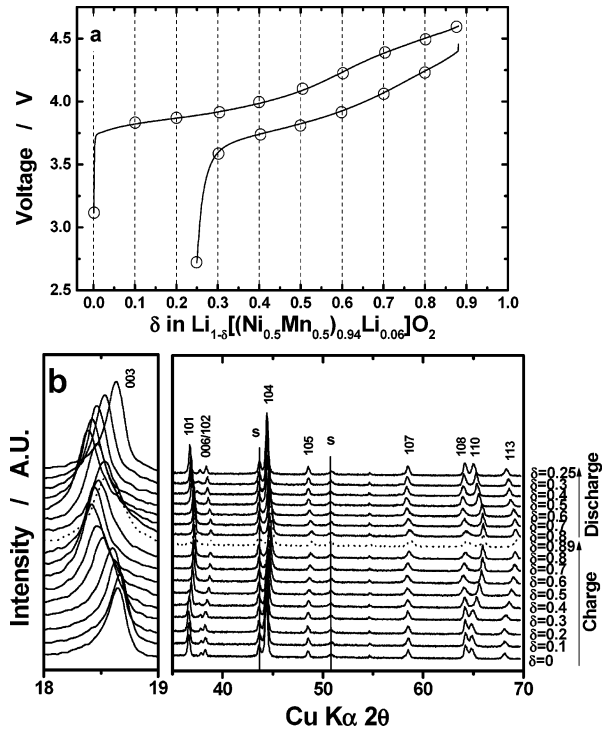


**Figure 9.** (a) Charge and discharge curves of the initial cycle for the Li/Li[(Ni$_{0.5}$Mn$_{0.5}$)$_{0.94}$Li$_{0.06}$]O$_2$ cell. In situ XRD measurements were carried out at the position marked by the circles. (b) In situ XRD patterns of Li$_{1-δ}$[(Ni$_{0.5}$Mn$_{0.5}$)$_{0.94}$Li$_{0.06}$]O$_2$ as a function of Li content during the first cycle. S donates a stainless exmet for loading active materials, and the exmet was used as the internal standard for calibration.

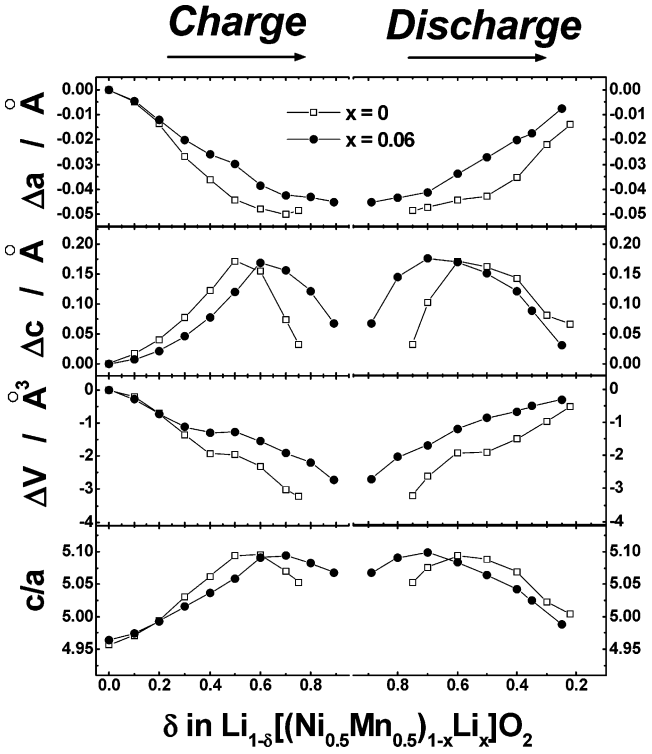


**Figure 10.** Variation in lattice parameters, unit cell volume, and *c*/*a* of Li$_{1-δ}$[(Ni$_{0.5}$Mn$_{0.5}$)$_{1-x}$Li$_x$]O$_2$ ($x = 0$ and 0.06).

enough for the steric effects to prevail over the electrostatic one. As can be seen in Figure 6, Li[(Ni$_{0.5}$Mn$_{0.5}$)$_{0.94}$Li$_{0.06}$]O$_2$ delivered an obviously higher capacity than Li[Ni$_{0.5}$Mn$_{0.5}$]O$_2$. Interestingly, the variation in the lattice constants by Li$^+$ extraction and insertion showed that the contraction of the

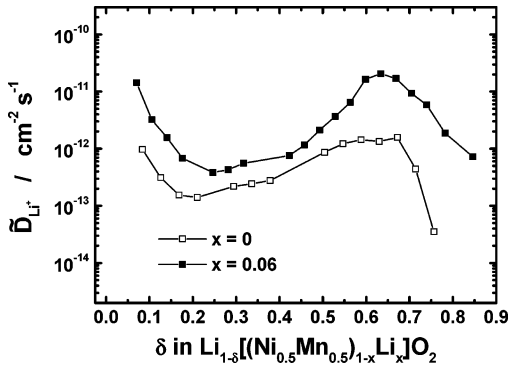


**Figure 11.** Chemical diffusion coefficient, $\tilde{D}_{Li^+}$, of Li$_{1-δ}$[(Ni$_{0.5}$Mn$_{0.5}$)$_{1-x}$Li$_x$]O$_2$ ($x = 0$ and 0.06).

host crystal structure was smaller even though the same amount of Li$^+$ was deintercalated for the Li-substituted Li[(Ni$_{0.5}$Mn$_{0.5}$)$_{0.94}$Li$_{0.06}$]O$_2$. This result would be due to the quite reduced structural disorder in the Li layer (2.6% cation mixing), which makes Li$^+$ movement easier in the interlayer, compared to that for Li[Ni$_{0.5}$Mn$_{0.5}$]O$_2$.

Chemical Li$^+$ diffusion was measured to understand the effect of the presence of elemental Li on the transition-metal layer for Li[(Ni$_{0.5}$Mn$_{0.5}$)$_{1-x}$Li$_x$]O$_2$ ($x = 0$ and 0.06) by GITT. $\tilde{D}_{Li^+}$ was calculated according to eq 1, derived from Huggins[20]

$$\tilde{D}_{Li^+} = \frac{4}{\pi}\left(\frac{V_m}{FA}\right)^2\left(\frac{I^0\frac{d\epsilon}{d\delta}}{\frac{d\epsilon}{dt^{1/2}}}\right)^2 \text{ for } t \ll \frac{\left(\frac{d}{2\pi}\right)^2}{\tilde{D}_{Li^+}} \qquad (1)$$

where $V_m$ is the molar volume, $F$ is the Faraday constant, $A$ is the contact area between the electrolyte and the sample, $I^0$ is the applied constant electric current, $d\epsilon/d\delta$ is the slope of the coulometric titration curve, and $(d\epsilon/dt)^{1/2}$ is the slope of the short-time transient voltage charge. The equation is valid for times shorter than the diffusion, $(d/2\pi)^2/\tilde{D}_{Li^+}$, where $d$ is the average diameter of the grains ($\sim$2 $\mu$m on average). The $\tilde{D}_{Li^+}$ values derived from eq 1 are based on the following assumption: the molar volume ($V_m$) remains unchanged with the change in Li content in the compounds, and a single-phase reaction occurred. As can be seen in Figure 11, the chemical diffusion coefficient of Li$^+$ for Li$_{1-δ}$[Ni$_{0.5}$Mn$_{0.5}$]O$_2$ ranged from $10^{-13}$ to $10^{-14}$ cm$^{-2}$ s$^{-1}$. By contrast, that for Li$_{1-δ}$[(Ni$_{0.5}$Mn$_{0.5}$)$_{0.94}$Li$_{0.06}$]O$_2$ was 10 times faster, showing $10^{-12}$ to $10^{-13}$ cm$^{-2}$ s$^{-1}$, compared with that for Li$_{1-δ}$[Ni$_{0.5}$Mn$_{0.5}$]O$_2$. From the beginning of Li$^+$ deintercalation, the chemical diffusivity drastically decreased on the order of about $10^{-1}$ cm$^{-2}$ s$^{-1}$ until $\delta = 0.2$ for both Li$_{1-δ}$[Ni$_{0.5}$Mn$_{0.5}$]O$_2$ and Li$_{1-δ}$[(Ni$_{0.5}$Mn$_{0.5}$)$_{0.94}$Li$_{0.06}$]O$_2$. Such an abrupt decrease is usually observed in the potential plateau.[21−24] In our case, the region corresponds to the voltage plateau at around 3.7−3.8 V in Figure 6a and b. Then, the diffusion becomes faster

(20) Weppner, W.; Huggins, R. A. *J. Electrochem. Soc.* **1977**, *124*, 1569.
(21) Bang, H. J.; Donepudi, V. S.; Prakash, J. *Electrochim. Acta* **2002**, *48*, 443.
(22) Kim, J.-H.; Myung, S.-T.; Yoon, C. S.; Oh, I.-H.; Sun, Y.-K. *J. Electrochem. Soc.* **2005**, *152*, A1707.
(23) Levi, M. D.; Salitra, G.; Markovsky, B.; Teller, H.; Aurbach, D.; Heider, U.; Heider, L. *J. Electrochem. Soc.* **1999**, *146*, 1279.
(24) Shaju, K. M.; Subba Rao, G. V.; Chowdari, B. V. R. *J. Electrochem. Soc.* **2004**, *151*, A1324.

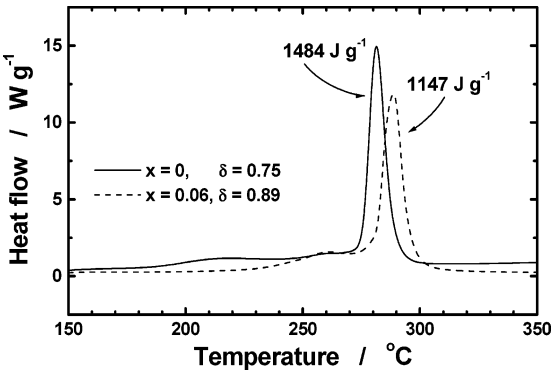


**Figure 12.** DSC traces of the Li/Li[$(Ni_{0.5}Mn_{0.5})_{1-x}Li_x$]$O_2$ ($x = 0$ and 0.06) cells at 4.6 V.

up to $\delta = 0.6$ in $Li_{1-\delta}[Ni_{0.5}Mn_{0.5}]O_2$ and $Li_{1-\delta}[(Ni_{0.5}Mn_{0.5})_{0.94}Li_{0.06}]O_2$. In this situation, as mentioned in Figure 10, ionic bonding character is predominant throughout the crystal structure so that the $Li^+$ diffusion could be faster due to the enlarged interlayer space. However, when the covalent bond which led to the abrupt shrinkage in the *c* axis prevails in the structure, the $Li^+$ diffusion coefficient decreased drastically, as seen in Figure 11. As mentioned in Table 3, cation mixing was greatly reduced by Li substitution for Ni and Mn in Li-$[(Ni_{0.5}Mn_{0.5})_{0.94}Li_{0.06}]O_2$. In general, the structural disorder significantly affects $Li^+$ diffusion because $Li^+$ diffusion always proceeds through the Li layer. In the case of the occurrence of cation mixing, the foreign element, $Ni^{2+}$, located in the Li layer blocks the $Li^+$ diffusion so that the rate becomes lower. Furthermore, the distance of Li−O was slightly longer for $Li[(Ni_{0.5}Mn_{0.5})_{0.94}Li_{0.06}]O_2$, as seen in Table 4. Wahihara et al.[25] reported that such a longer Li−O distance has relatively weaker Li−O bonding, and it simultaneously makes $Li^+$ diffusion easier. More recently, Shizuka et al.[26] reported that the electrical conductivity of $Li_{1+y}Ni_xCo_{1-2x}Mn_xO_2$ ($0.33 \le x \le 0.475$ and $0 \le y \le 0.2$) was greatly improved by Li incorporation into the transition-metal layer. From these points of view, $Li[(Ni_{0.5}Mn_{0.5})_{0.94}Li_{0.06}]O_2$ could have enhanced $Li^+$ diffusivity compared to $Li[Ni_{0.5}Mn_{0.5}]O_2$.

Figure 12 exhibits DSC profiles of the highly delithiated $Li_{0.25}[Ni_{0.5}Mn_{0.5}]O_2$ and $Li_{0.11}[(Ni_{0.5}Mn_{0.5})_{0.94}Li_{0.06}]O_2$. Both materials exhibited simple DSC curves with onset temperatures of exothermic reactions higher than 270 °C. Though a larger amount of $Li^+$ was extracted from $Li[(Ni_{0.5}Mn_{0.5})_{0.94}Li_{0.06}]O_2$ compared to $Li[Ni_{0.5}Mn_{0.5}]O_2$, which means that $Li_{1-\delta}[(Ni_{0.5}Mn_{0.5})_{0.94}Li_{0.06}]O_2$ is in a higher charged state than $Li_{1-\delta}[Ni_{0.5}Mn_{0.5}]O_2$ at 4.6 V, the small amount of Li incorporation into the transition-metal layer resulted in a pretty reduced heat generation of about 1147 W $g^{-1}$ and increased the main exothermic temperature to 290 °C, as seen in Figure 12. Therefore, it is concluded that structural stabilization by Li substitution for the transition-metal sites brought about the depression of significant exothermic activity and reduced the heat-generation at a highly delithiated state.

## Conclusion

In an attempt to synthesize highly crystalline $Li[Ni_{0.5}Mn_{0.5}]O_2$, the starting emulsion was prepared varying the starting Li/(Ni + Mn) ratio from 1 to 1.25. When the ratio was 1, the integrated intensity of $I_{003}/I_{104}$ was less than 1 due to the evaporation of elemental Li at a high temperature, 950 °C. Increasing the Li/(Ni + Mn) ratio to 1.25, we could successfully obtain stoichiometric $Li[Ni_{0.5}Mn_{0.5}]O_2$ and $Li_{1.13}[Ni_{0.5}Mn_{0.5}]O_{2+z}$ by controlling the amount of evaporation of Li at 950 °C. Neutron diffraction of Rietveld refinements showed that there are no secondary phases such as $Li_2O$, $Li_2CO_3$, and $Li_2MnO_3$ for the final products, and the tentative $Li_{1.13}[Ni_{0.5}Mn_{0.5}]O_{2+z}$ composition can be written as $Li[(Ni_{0.5}Mn_{0.5})_{0.94}Li_{0.06}]O_2$ by following the α-$NaFeO_2$ layer structure. Combining neutron diffraction with XANES studies, we found that the excess Li located at the transition-metal sites significantly improved the structural ordering of both Li and transition-metal sites for $Li[(Ni_{0.5}Mn_{0.5})_{0.94}Li_{0.06}]O_2$ and increased the average oxidation state of Ni, compared to $Li[Ni_{0.5}Mn_{0.5}]O_2$. Such improved structural integrity for $Li[(Ni_{0.5}Mn_{0.5})_{0.94}Li_{0.06}]O_2$ showed a much higher capacity and superior cyclability, compared to $Li[Ni_{0.5}Mn_{0.5}]O_2$, which possesses relatively higher cation mixing in the crystal structure. In situ XRD observations confirmed that the variation in the *a* and *c* axes was also smaller for $Li[(Ni_{0.5}Mn_{0.5})_{0.94}Li_{0.06}]O_2$, which would be ascribed to the structural stabilization by Li substitution for Ni and Mn sites for $tLi[(Ni_{0.5}Mn_{0.5})_{0.94}Li_{0.06}]O_2$. The improved physical properties also enhanced the chemical diffusivity of $Li^+$ and led to good thermal safety characteristics at a highly oxidized state, as confirmed by differential scanning calorimetry.

**Acknowledgment.** The authors thank S. Takahashi, A. Ueyama, Y. Fujisawa, from Iwate University, and R. Kodama, from Tokyo University of Science, for their helpful assistance in the experimental work. This study was financially supported in 2000−2004 by the program "Development of Rechargeable Lithium Battery with High Energy/Power Density for Vehicle Power Sources" of the Industrial Technology Research Grant Program from the New Energy and Industrial Technology Development Organization (NEDO), Japan.

CM052704J

(25) Song, D.; Ikuta, H.; Uchida, T.; Wahihara, M. *Solid State Ionics* **1999**, *117*, 151.
(26) Shizuka, K.; Kobayashi, T.; Okahara, K.; Okamoto, K.; Kanzaki, S.; Kanno, R. *J. Power Sources* **2005**, *146*, 589.